The ns12.9 accessory protein of human coronavirus OC43 is a viroporin involved in virion morphogenesis and pathogenesis

Ronghua Zhang,[a,b] Kai Wang,[b*] Xianqiang Ping,[b] Wenjing Yu,[b] Zhikang Qian,[b] Sidong Xiong,[a#] Bing Sun[b,c#]

Jiangsu Key Laboratory of Infection and Immunity, Institutes of Biology and Medical Sciences, Soochow University, Suzhou, China[a]; Key Laboratory of Molecular Virology and Immunology, Institut Pasteur of Shanghai, Shanghai Institutes for Biological Sciences, Chinese Academy of Sciences, Shanghai, China[b]; State Key Laboratory of Cell Biology, Institute of Biochemistry and Cell Biology, Shanghai Institutes for Biological Sciences, Chinese Academy of Sciences, Shanghai, China[c]

Running title: ns12.9 promotes virus morphogenesis and pathogenesis

#Address correspondence to Sidong Xiong, sdxiongfd@126.com, or Bing Sun, bsun@sibs.ac.cn.

*Current address: The College of Basic Medical Sciences, Chongqing Medical University, Chongqing, China

ABSTRACT

An accessory gene between the S and E gene loci is contained in all coronaviruses (CoVs), and its function has been studied in some coronaviruses. This gene locus in human coronavirus OC43 (HCoV-OC43) encodes the ns12.9 accessory protein; however, its function during viral infection remains unknown. Here, we engineered a recombinant mutant virus lacking the ns12.9 protein (HCoV-OC43-Δns12.9) to characterize the contributions of ns12.9 in HCoV-OC43 replication. The ns12.9 accessory protein is a transmembrane protein and forms ion channels in both *Xenopus* oocytes and yeast through homo-oligomerization, suggesting that ns12.9 is a newly recognized viroporin. HCoV-OC43-Δns12.9 presented at least 10-fold reduction of viral titer *in vitro* and *in vivo*. Intriguingly, exogenous ns12.9 and heterologous viroporins with ion channel activity could compensate the production of HCoV-OC43-Δns12.9, indicating that the ion channel activity of ns12.9 plays a significant role in the production of infectious virions. Systematic dissection of single-cycle replication revealed that ns12.9 protein had no measurable effect on virus entry, subgenomic messenger RNA (sgmRNA) synthesis and protein expression. Further characterization revealed that HCoV-OC43-Δns12.9 was less efficient in virion morphogenesis than recombinant wild-type virus (HCoV-OC43-WT). Moreover, reduced viral replication, inflammatory response and virulence in HCoV-OC43-Δns12.9-infected mice were observed compared with HCoV-OC43-WT-infected mice. Taken together, our results demonstrated that the ns12.9 accessory protein functions as a viroporin, and is involved in virion morphogenesis and

41 the pathogenesis of HCoV-OC43 infection.

IMPORTANCE

HCoV-OC43 was isolated in the 1960s and is a major agent of the common cold. The functions of HCoV-OC43 structural proteins have been well studied, but few studies have focused on its accessory proteins. In the present study, we demonstrated that the ns12.9 protein is a newly recognized viroporin, and the ns12.9 gene knockout virus (HCoV-OC43-Δns12.9) presents a growth defect *in vitro* and *in vivo*. We identified the important functions of the ns12.9 viroporin in virion morphogenesis during HCoV-OC43 infection. Furthermore, mice infected with HCoV-OC43-Δns12.9 exhibited reduced inflammation and virulence accompanied by a lower titer in the brain compared with wild-type infected mice, suggesting the ns12.9 viroporin influences virus pathogenesis. Therefore, our findings revealed that the ns12.9 viroporin facilitates the virion morphogenesis to enhance viral production, and these results provided a deeper understanding of HCoV-OC43 pathogenesis.

INTRODUCTION

The coronaviruses (CoVs) belong to the *Coronaviridae* family of the order *Nidovirales* and are distributed widely among animals, birds and humans (1). Members of the CoVs are further classified into four genera as follows: *Alphacoronavirus*, *Betacoronavirus*, *Gammacoronavirus* and *Deltacoronavirus* (2). Human coronavirus OC43 (HCoV-OC43) was isolated from a patient with upper respiratory tract disease in the 1960s and classified into the *Betacoronavirus* genus (3). HCoV-OC43 causes mild upper respiratory infection and is identified as a major etiological agent of the common cold (4). Additionally, this virus exhibits neuroinvasive properties that lead to neurological diseases (5-7).

The genome of CoVs is a single-stranded, positive-sense RNA that is 27 to 32 kb in length, and the genome is 5'-capped and 3'-polyadenylated. Approximately two-thirds of the 5'-proximal genome consists of the ORF1a/b replicase gene, whereas the remainder of the genome encodes several accessory proteins and the following four major structural proteins: spike (S), envelope (E), membrane (M) and nucleocapsid (N) proteins (1). The replicase gene encodes two large polyproteins, namely pp1a and pp1ab, which form a set of nonstructural proteins with autoproteolytic cleavage. These nonstructural proteins are essential for viral transcription, RNA replication and pathogenesis (8). The S, E and M proteins are transmembrane proteins embedded in the viral lipid envelope. The S protein interacts with the host corresponding receptors to mediate the virus entry process (9-12). The E and M proteins are critical for viral morphogenesis. Studies have shown that expression of the E protein with M protein is sufficient to form virus-like particles (VLPs)

in vitro (13-15). The major function of the N protein involves binding the viral RNA to form a helical nucleocapsid that is surrounded by the viral envelope (1). The members of lineage A of genus *Betacoronavirus*, including HCoV-OC43, bovine coronavirus (BCoV), mouse hepatitis virus (MHV) and HCoV-HKU1, possess a hemagglutinin-esterase (HE) gene between the ORF1a/b and S gene. The HE protein is considered as the fifth structural protein that incorporates into the viral envelope, and this protein participates in the entry and release process of viral infection (16, 17).

In addition to the structural genes, the genome of CoVs contains accessory genes interspersed among the other genes. The accessory proteins of various CoVs are involved in viral pathogenesis and virulence (18-21), and some of these proteins are dispensable for viral replication (22-24). CoVs accessory genes exhibit individual specificity with numbers varying from one (e.g., HCoV-NL63) to eight (e.g., SARS-CoV). Strikingly, an accessory gene between the S and E gene loci is contained in all CoVs, suggesting that it may play important and conserved roles during CoVs infection (1). In our previous study, we found that this accessory protein of SARS-CoV (SARS-3a) and HCoV-229E (229E-ORF4a) forms ion channels (25, 26). These ion channel proteins are identified as viroporins, which is a viral protein family that forms ion channels to permeabilize the membrane and regulate viral infection (27).

Genome nucleotide sequence analysis indicates that the accessory gene between S and E gene loci of HCoV-OC43 encodes a potential protein with a molecular weight of 12.9 kDa, and this protein is named ns12.9 (28). However, the function of the ns12.9

accessory protein during HCoV-OC43 infection is not well known. In the present study, we revealed that the ns12.9 accessory protein is a new member of the viroporins and facilitates the virion morphogenesis to enhance viral production. To our knowledge, this is the first study to define the function of an accessory protein in virion formation stage during CoVs infection. Moreover, HCoV-OC43-Δns12.9 is attenuated in virulence, suggesting that HCoV-OC43-Δns12.9 may be developed as a candidate vaccine to protect against HCoV-OC43 infection.

MATERIALS AND METHODS

Cells and viruses. HEK293T, BHK-21 and RD cells were cultured in Dulbecco's modified Eagle's medium (DMEM, Gibco) supplemented with 10% fetal bovine serum (FBS, Gibco), penicillin (100 U/mL) and streptomycin (100 μg/mL) in a humidified atmosphere of 5% CO_2 at 37°C. The recombinant wild-type HCoV-OC43 (HCoV-OC43-WT) and ns12.9 knockout HCoV-OC43 mutant (HCoV-OC43-Δns12.9) was rescued from the infective cDNA clones pBAC-OC43-WT and pBAC-OC43-Δns12.9, respectively. Separate laminar flow hoods and CO_2 incubators were used during the experiments to avoid possible cross-contamination. Mutation within the ns12.9 gene of HCoV-OC43-Δns12.9 remained very stable *in vitro* and *in vivo*, since no changes were found in ns12.9 gene during the course of experiments. The recombinant HCoV-OC43-WT and HCoV-OC43-Δns12.9 viral stocks (10^6 $TCID_{50}$/mL) were maintained at -80°C.

Plasmids construction. Sequences encoding SARS-3a, NL63-ORF3, 229E-ORF4a, OC43-ns12.9, influenza A virus (IAV) M2, hepatitis C virus (HCV) p7 and human enterovirus 71 (EV71) 2B were amplified by PCR and cloned into the pCAGGS vector (a kind gift from Jun-ichi Miyazaki, Osaka University, Japan) with a C-terminal HA tag or Flag tag for expression. ns12.9-HA sequence was cloned into pNWP vector (a kind gift from Jian Fei, Shanghai Institute of Biological Science, China) for cRNA *in vitro* transcription and cloned into a yeast expression vector pYES2 (a kind gift from Wei Song, Shanghai Institute of Biological Science, China) for yeast potassium uptake

complementation assay. The infective full-length HCoV-OC43 cDNA clone pBAC-OC43-WT was kindly provided by Pierre J. Talbot (INRS-Institut Armand-Frappier, Québec, Canada). The pBAC-OC43-Δns12.9 cDNA clone was constructed in our laboratory following a previously described protocol (29). Briefly, a cassette containing a stop codon at the fourth amino acid of the ns12.9 gene followed by the sequence with a selective kanamycin marker that flanked by flippase recognition target (FRT) sites was amplified from the pYD-C191 plasmid with a pair of 70-nt primers as follows: forward primer OC43-FRT-F, 5'-CTAGCATTTGTTAAAGTTCTTAAGGCCACGCCCTATTAATGGACATTTG**A**AAGG ACGACGACGACAAGTAA-3'; and reverse primer OC43-FRT-R, 5'-TCTGAGACATTAAAACCGTTAATATAACGGAGATATTTCTTCTCAGGTCTACCA CGTCGTGGAATGCCTTC-3'. The underlined 50-nt sequences were homologous to the viral genome sequences immediately upstream or downstream of the mutant nucleotide position (bold). This cassette was subsequently recombined into the pBAC-OC43-WT cDNA clone by linear recombination in the SW102 bacterial strain. Resulting transformants were selected on LB plates with chloramphenicol and kanamycin to identify the mutant cDNA clone. Finally, arabinose was added to the culture media to induce Flp recombinase expression to remove the kanamycin sequence. Therefore, the resulting pBAC-OC43-Δns12.9 cDNA clone contained a single-nucleotide mutation at position 12 of the ns12.9 gene in addition to an 82-nt segment insertion. This 82-nt sequence consisted of one FRT site (boxed) and an EcoRI restriction site (italic) as

follows:

AAGGACGACGACGACAAGTAAGAAGTTCCTATTCTCTAGAAAGTATAGGAACT TC*GAATTC*GAAGGCATTCCACGACGTGGT. All plasmids were verified by restriction digestion analysis and direct sequencing.

Antibodies. The anti-HA mouse monoclonal antibody (MMS-101P) was purchased from Covance. Anti-HA (H6908) and anti-Flag (F7425) rabbit polyclonal antibodies were purchased from Sigma. The Alexa Fluor 488-conjugated goat anti-mouse antibody (A11029) and Cy3-conjugated goat anti-rabbit antibody (111-165-045) were obtained from Molecular Probes. The OC43-N mouse monoclonal antibody (MAB9012) was purchased from Merck Millipore. The horseradish peroxidase (HRP)-conjugated goat anti-mouse IgG antibody and HRP-conjugated goat anti-rabbit IgG antibody were obtained from the Antibody Research Center (Shanghai Institute of Biochemistry and Cellular Biology, Chinese Academy of Sciences, Shanghai, China). The ERGIC53 antibody (H-245), a rabbit polyclonal antibody against the endoplasmic reticulum/Golgi intermediate compartment (ERGIC), was obtained from Santa Cruz Biotechnology. The mouse IL-1β (DY401) and IL-6 (DY406) ELISA kits were purchased from R&D systems.

Confocal microscopy. Cells were washed with PBS at 24 hours after infection or transfection, fixed with 4% paraformaldehyde (PFA) and then permeabilized with 0.3% Triton X-100. The cells were blocked with 2% bovine serum albumin (BSA) and immunolabeled with primary antibodies for 2 hours at room temperature. Cells were

washed with phosphate-buffered saline (PBS) and incubated with Cy3-conjugated goat anti-rabbit antibody or Alexa Fluor 488-conjugated goat anti-mouse antibody for 1 hour. Nuclei were stained with DAPI (D9542, Sigma-Aldrich). Colocalization studies were examined using a Leica TCS SP5 confocal microscope (Leica Microsystems).

Coimmunoprecipitation and western blot. Transfected cells were lysed in RIPA buffer (50 mM Tris-HCl pH 7.4, 150 mM NaCl, 1% NP-40, 0.25% Na-deoxycholate, 1 mM EDTA) with protease inhibitor (Roche, Switzerland). Cell lysates were centrifuged at 15,000 x *g* for 20 min at 4°C, and the supernatant was incubated with ANTI-FLAG M2 affinity gel (A2220, Sigma) or anti-HA agarose (A2095, Sigma) at 4°C overnight. The gels or agaroses were then washed 5 times with RIPA buffer and lysed in sodium dodecyl sulfate (SDS) loading buffer (50 mM Tris–HCl pH 6.8, 2% SDS, 10% glycerol, 1% β-mercaptoethanol, and 0.1% bromophenol blue).

The proteins were separated by 15% SDS-PAGE and transferred to nitrocellulose membranes (Bio-Rad). Membranes were blocked with 5% skim milk for 1 hour and incubated with primary antibody overnight at 4°C. After washes with TBST (50 mM Tris, 150 mM NaCl, and 0.1% Tween-20, pH 7.5), the membranes were further incubated for 1 hour with HRP-conjugated secondary antibody. The protein expression was visualized using SuperSignal West Pico Chemiluminescent Substrate (Thermo Scientific).

Flow cytometry. The transfected cells or infected cells were collected and washed with PBS. Cells were then fixed with 4% PFA, immunolabeled with primary antibody and incubated with an Alexa Fluor 488-conjugated goat anti-mouse antibody. Cells were

resuspended in PBS and analyzed by flow cytometry (FACS-LSRII, BD Biosciences). Data analysis was performed using FlowJo software (TreeStar).

Electrophysiological measurements. The ns12.9-HA cRNA was synthesized using the mMESSAGE mMACHINE high-yield capped RNA transcription SP6 kit (Ambion, USA) from the pNWP-ns12.9-HA plasmid. Healthy oocytes in stage V to VI were injected with 30 ng of cRNA and incubated at 18°C in an ND-96 solution (96 mM NaCl, 2 mM KCl, 1.8 mM CaCl2, 1 mM MgCl2, 2.5 mM pyruvate and 5 mM HEPES, adjusted to pH 7.4 with NaOH). Two-electrode voltage clamp was used to record the currents mediated by ns12.9 protein from the membranes of *Xenopus* oocytes as described previously (26). Briefly, the standard voltage-clamp protocol consisted of rectangular voltage pulses from -150 to +30 mV in 10-mV increments applied from a holding voltage of -60 mV. During the current recording, the oocytes were bathed in the ORi solution (90 mM NaCl, 2 mM KCl, 2 mM CaCl2 and 5 mM HEPES, adjusted to pH 7.4 with NaOH) at room temperature. Current recording and analysis were performed with pClamp 10.0 software (Axon Instruments).

Yeast potassium uptake complementation assay. Either the empty pYES2 or pYES2-ns12.9-HA vector were transformed into a potassium uptake-deficient yeast strain W303 R5421 (*ura*3-52 *his*3Δ200 *leu*2Δ1 *trp*1Δ1 *ade*2 *trk1*Δ::HIS3 trk2Δ::HIS3) (a kind gift from Richard F. Gaber, Northwestern University, USA) with the lithium acetate procedure. The pYES2 vector contains a URA3 gene as a selectable marker for positive transformants in *ura* negative hosts. The exogenous gene is controlled by the *GAL1*

promoter and its expression was induced in the presence of galactose. Complementation of the potassium uptake-deficient yeast was performed as previously described (25). Briefly, yeasts from the same stock were diluted and grown in parallel on YNB *ura* negative plates supplemented with 100 mM KCl or 0.2 mM KCl. Plates were kept at 30 °C for 3-4 days.

Rescue of recombinant HCoV-OC43 viruses. BHK-21 cells were seeded in 6-well plates and transfected with the 5 µg of wild-type or mutant cDNA clone using Lipofectamine 2000 (Invitrogen) according to the manufacturer's protocol. The culture medium was replaced by DMEM supplemented with 2% FBS 24 hours after transfection and maintained at 33°C for an additional 72 hours. Cell supernatants containing recombinant virus corresponding to the cDNA clone were amplified in RD cells and quantified by the immunoperoxidase assay (IPA).

Titration of rescued virus using IPA. The titers of infectious HCoV-OC43 virions were determined by IPA as previously reported (30, 31). Briefly, RD cells were seeded in 96-well plates and infected with each virus in a serial dilution of 10^{-1} to 10^{-7}. Cells were incubated for 4 days, and the cells were then fixed with 4% PFA and permeabilized with 0.3% Triton X-100. The monoclonal mouse antibody specific for the HCoV-OC43 N protein and HRP-conjugated goat anti-mouse IgG antibody were used as the primary and secondary antibodies, respectively. The viral antigens were visualized using TrueBlue Peroxidase Substrate (KPL), and the viral titers were calculated by the Karber method. For intracellular virions, cells were disrupted by three cycles of freeze-thawing in dry ice

and a 37°C water bath, and the viral titers were then quantified as described above.

Viral growth kinetics. RD or BHK-21 cells were plated into 12-well plates and infected at a multiplicity of infection (MOI) of 0.1. Media (2 mL) was added to each well, and 300 µl of supernatant was collected at 0, 4, 24, 48, 72, 96, 120 and 144 hours post-infection (hpi). Viral titers were determined by IPA as described above.

RNA extraction and quantitative RT-PCR. Viral genomic RNA was extracted from cell supernatants using the TIANamp Virus RNA Kit (TIANGEN) following the manufacturer's instructions. The ns12.9 gene was checked using the primers as follows: forward primer ns12.9-F, 5'-GGTGGTTGTTGTGATGATTATACTGGATACC-3' and reverse primer ns12.9-R, 5'-CCACTACAACTATTGTAACCAATAAACAAATGG-3'. Total RNA from virus-infected cells was extracted using TRIzol reagent (Invitrogen). RNA (1 µg) was then used for reverse transcription using the ReverTra Ace qPCR RT Kit (Toyobo). The target gene described above was amplified by PCR from the cDNA. The copies of genomic RNA and subgenomic messenger RNA (sgmRNA) in infected cells were determined by quantitative real time PCR (qRT-PCR) using SYBR Green Realtime PCR Master Mix (Toyobo). β-actin was used as an internal control. All the primers are presented in Table 1.

Transmission Electron Microscopy. RD Cells were infected with recombinant WT or Δns12.9 viruses at a MOI of 1 for 24 hours. The cells were washed with PBS and fixed with 2% glutaraldehyde overnight at 4°C. The samples were then treated with 2% osmium tetroxide for 1 hour, dehydrated gradually through an ethanol series (30, 50, 70,

90 and 100%) and embedded in Epon812 resin. The infiltrated samples were polymerized at 60°C for 48 hours. Ultrathin sections (70 nm) of the cells were produced using an EM UC6 ultramicrotome (Leica) and stained with 2% uranyl acetate and 1% lead citrate. The sections were analyzed with a Tecnai Spirit transmission electron microscope (FEI).

Mice and infection. Specific-pathogen-free BALB/c mice were obtained from the Jackson Laboratory. Mice were maintained at the Animal Care Facility of the Chinese Academy of Sciences. Groups of 10-day-old mice were intranasally inoculated with 5 μl of the HCoV-OC43-WT or HCoV-OC43-Δns12.9 viral stock (32). The infected mice were monitored daily for weight loss and survival. Four mice of each group were sacrificed at 2, 4 and 6 days post-infection (dpi), and the brain tissues were collected. All protocols complied with the Institutional Animal Care and Use Committee guidelines. The brain tissues were homogenized in 30% (wt/vol) PBS and centrifuged at 12,000 × *g* for 20 min at 4°C, and the supernatants were then collected to detect the viral titers or cytokine levels.

Enzyme-linked immunosorbent assay (ELISA). Mouse proinflammatory cytokines were measured by ELISA according to the manufacturer's instructions.

RESULTS

The ns12.9 accessory protein acts as a viroporin. Viroporins are a group of small hydrophobic proteins that tend to oligomerize to form hydrophilic pores or ion channels in cellular membrane (27). Since we previously demonstrated that the SARS-3a and 229E-ORF4a are viroporins, we wanted to evaluate whether this accessory protein ns12.9 in HCoV-OC43 acts as a viroporin. Analysis of the hydrophobicity of ns12.9 protein sequence with the Kyte-Doolittle hydropathy plot (33) revealed that ns12.9 contains a hydrophobic segment with 21 amino acids, which could be a potential transmembrane domain (TMD) of integral membrane proteins (Fig. 1A). The plasma membrane localization of ns12.9 was then tested with immunofluorescence staining. As shown in Fig. 1B and C, C-terminally HA-tagged ns12.9 was detected at the cell membrane surfaces of non-permeabilized cells, suggesting that ns12.9 is a transmembrane protein with an intracellular N terminus and an extracellular C terminus.

We next sought to investigate whether ns12.9 could form homo-oligomers. Coimmunoprecipitation assays were performed with 293T cells transiently transfected with plasmids encoding HA-tagged and Flag-tagged ns12.9. Notably, coimmunoprecipitation of ns12.9-HA with ns12.9-Flag was detected (Fig. 1D), indicating that ns12.9 is able to oligomerize. To confirm the self-oligomerization of ns12.9, the ns12.9 oligomers were analyzed in anti-HA immunoprecipitates. As shown in Fig. 1E, the monomer and oligomers of ns12.9 were separated by SDS-PAGE, confirming the homo-oligomerization of ns12.9.

Journal of Virology

Finally, to assess the ion channel activity of ns12.9, membrane currents of ns12.9 cRNA injected *Xenopus* oocytes were recorded using two electrode voltage clamp (TEVC). A dramatic increase of membrane conductance was detected in the ns12.9-expressing oocytes compared with the control oocytes (Fig. 1F and G). In addition, a yeast complementation assay was performed using the potassium uptake-deficient yeast, which grows poorly on low-potassium medium. As shown in Fig. 1H, the growth of ns12.9-expressing transformants could be rescued on the low-potassium (0.2 mM) medium, whereas empty transformants only grew on the high-potassium (100 mM) medium. Therefore, the ns12.9 forms ion channels in *Xenopus* oocytes and yeast.

Collectively, these observations suggest that the ns12.9 accessory protein acts as a viroporin in that it oligomerizes in the cell membrane to form ion channels.

Rescue of the ns12.9-knockout HCoV-OC43 mutant. To investigate the function of the ns12.9 during HCoV-OC43 infection, a recombinant mutant virus defective in the ns12.9 gene was rescued by reverse genetics. For this purpose, we constructed an ns12.9 gene knockout cDNA clone (pBAC-OC43-Δns12.9), in which the fourth codon of ns12.9 coding sequence was changed to a stop codon. In addition, an 82-nt segment was inserted behind the mutant stop codon to avoid the occurrence of genetic reversion (Fig. 2A). The pBAC-OC43-Δns12.9 mutant cDNA clone was engineered from the infective wild-type clone (pBAC-OC43-WT) by homologous recombination and examined by the digestion with the EcoRI restriction enzyme and direct sequencing (Fig. 2B and data not shown). To determine whether the virus was rescued from the cDNA clone in transfected BHK-21

312 cells, supernatants from transfected cells were harvested and used to infect the RD cells.
313 After three rounds of amplification in RD cells, the existence of viral RNA and N protein
314 in supernatants and RD cells, respectively, were analyzed. As an 82-nt segment was
315 inserted in ns12.9 gene within pBAC-OC43-Δns12.9, the ns12.9 gene amplified from
316 HCoV-OC43-Δns12.9-infected cells was slightly larger than that amplified from
317 HCoV-OC43-WT-infected cells (Fig. 2C). In addition, similar to the wild-type virus, the
318 OC43-N proteins were detectable in the mutant virus-infected RD cells (Fig. 2D). These
319 results suggest that the HCoV-OC43-Δns12.9 virus was successfully rescued by the
320 mutant cDNA clone.

321 **HCoV-OC43-Δns12.9 is defective in growth *in vitro*.** To evaluate the role of the
322 ns12.9 viroporin contributing to viral production, we analyzed the growth kinetics of the
323 recombinant HCoV-OC43-WT and HCoV-OC43-Δns12.9 mutant viruses in the BHK-21
324 and RD cells. In BHK-21 cells, the wild-type virus replicated efficiently and reached the
325 maximal titer of approximately $10^{8.0}$ $TCID_{50}$/mL at 144 hpi. In contrast, the peak titer of
326 the HCoV-OC43-Δns12.9 virus was approximately $10^{6.6}$ $TCID_{50}$/mL at 120 hpi, which
327 was approximately 25-fold reduced compared with the wild-type virus (Fig. 3A). In RD
328 cells, although the wild-type and mutant viruses exhibited a similar growth pattern with
329 maximal titers between 96 and 144 hpi, the wild-type viral titer was 10-fold increased
330 compared with the mutant virus (Fig. 3B). These data indicate that the ns12.9 viroporin is
331 important for the viral propagation in cell cultures.

332 **Transient expression of the ns12.9 and this accessory protein from other**

coronaviruses complements HCoV-OC43-Δns12.9. The reduced viral yield of HCoV-OC43-Δns12.9 in cultured cell lines suggested that the ns12.9 viroporin is important for viral infection. To explore whether the defect is due to the abolishment of ns12.9 viroporin expression, we performed a transient complementation assay. An ns12.9 protein expression vector was constructed and its expression level was detected by western blot analysis (Fig. 4A). In this assay, the empty or ns12.9 expression vector was transfected into RD cells followed by HCoV-OC43-WT or HCoV-OC43-Δns12.9 infection, and the supernatants were collected to determine virus titers. Compared with the empty vector-transfected cells, ns12.9-expressing cells exhibited a significant enhancement of viral production for both HCoV-OC43-Δns12.9 and HCoV-OC43-WT viruses (Fig. 4B). These results confirm that the ns12.9 viroporin plays an important role in the production of infectious virus.

Since the accessory gene between the S and E gene loci is contained in all CoVs, we sought to test whether this accessory protein of other HCoVs could compensate the production of HCoV-OC43-Δns12.9. Vectors expressing the SARS-3a, 229E-ORF4a and NL63-ORF3 were constructed, and their expression levels were detected by western blot analysis (Fig. 4C). As shown in Fig. 4D, The cells transfected with these vectors led to a significant increase in the viral production compared to the cells transfected with empty vector, thereby suggesting that these accessory proteins might have a conserved function during HCoVs infection.

Transient expression of other viroporins complements HCoV-OC43-Δns12.9.

Viroproins are small ion channel proteins encoded by a wide range of viruses and involved in different aspects of virus life cycle (27, 34, 35). Therefore, we assessed whether other viroporins could impact HCoV-OC43 infection. Three well researched viroporins, IAV-M2, HCV-p7 and EV71-2B, were selected and analyzed (Fig. 5A). These viroporins expressing vectors were transfected into RD cells followed by HCoV-OC43-Δns12.9 infection. Similar to the ns12.9-expressing cells, the M2 and 2B-expressing cells showed a significant enhancement of viral production. However, the p7 viroporin failed to compensate the HCoV-OC43-Δns12.9 in replication (Fig. 5B), suggesting a distinct function between ns12.9 and p7 during viral infection.

To specifically analyze the relevance of ion channel activity in viral production, mutations or deletions within the putative TMD of ns12.9 were introduced to construct ns12.9 mutant that lacks ion channel activity. However, these mutants failed to change its ion conductivity or to localize at the cell membrane (data not shown). Given that the production of HCoV-OC43-Δns12.9 was compensated in cells expressing the M2 in *trans*, we attempted to evaluate the contribution of viroporin ion conductivity to viral production by the complementation assay of M2Δ29-31 mutant (Fig. 5C), whose ion channel activity is completely disrupted as a deletion of three amino acids 29-31 in the M2 TMD (36, 37). As shown in Fig. 5D, transient expression of M2, but not the M2Δ29-31 mutant complemented HCoV-OC43-Δns12.9 in RD cells, indicating that the ion channel activity of viroporins is closely related to the production of HCoV-OC43.

ns12.9 does not impact viral entry, sgmRNA synthesis and protein expression. To

define the step of the virus life cycle where the ns12.9 viroporin functions, the viral single replication cycle was dissected and analyzed systematically. We first investigated the viral entry process. The efficiency of HCoV-OC43-WT and HCoV-OC43-Δns12.9 infection at 0.5 and 1.5 hpi was analyzed by flow cytometry. As shown in Fig. 6A, similar percentages of N-positive cells were observed in cells infected with the wild-type and mutant viruses, indicating that the ns12.9 protein is not required for the entry process. To further assess genomic replication kinetics, the level of genomic RNA (gRNA) was evaluated by qRT-PCR at early time points in the wild-type and mutant virus-infected RD cells. Similar levels of gRNA was observed in cells infected with both viruses (Fig. 6B), thereby suggesting that the ns12.9 viroporin does not affect genomic replication of HCoV-OC43.

As a member of the order *Nidovirales*, coronavirus generates a series of smaller, sgmRNAs that serve as the messenger RNAs for viral protein synthesis. To address whether the knockout of ns12.9 alters sgmRNA synthesis, all HCoV-OC43 sgmRNAs were measured by qRT-PCR. To amplify the sgmRNAs, a leader sequence was selected as a forward primer, and reverse primers were complementary to each gene sequence (Table 1). As shown in Fig. 6C, no significant change was measured in the amount of each sgmRNA between the wild-type and mutant virus, except for ns12.9 sgmRNA. One possible explanation for this observation is that the qPCR amplification efficiency of ns12.9 gene was suppressed by the extended 82-nt segment in the ns12.9 gene. Because the production of sgmRNA was not affected by ns12.9, deletion of the ns12.9 protein may

not influence viral protein synthesis. To confirm that viral protein synthesis was independent of ns12.9, the main structure protein N was selected, and its expression during the time course of infection was detected by western blot analysis. As expected, comparable level of N protein expression were observed for cells infected with wild-type and mutant HCoV-OC43 viruses (Fig. 6D).

Taken together, these data demonstrate that the ns12.9 viroporin is dispensable for the early steps and protein expression of HCoV-OC43 infection.

ns12.9 is involved in the virions morphogenesis. To address whether ns12.9 regulates the late stages of virus life cycle, we first examined the subcellular localization of ns12.9 during HCoV-OC43 infection. The ns12.9 was evenly distributed in the cytoplasm and nucleus of RD cells when ns12.9 was exclusively expressed (Fig. 7, upper panels). Surprisingly, in wild-type or mutant virus infected RD cells, ns12.9 was localized at ERGIC (Fig. 7, middle and lower panels), the compartment where CoVs assemble and bud intracellularly during viral infection (1). These observations indicate that other viral factors are involved in the localization of ns12.9 during HCoV-OC43 infection.

Given that the ns12.9 viroporin is dispensable for the early steps of virus life cycle and is localized at ERGIC during viral infection, we hypothesized that ns12.9 may have a potential effect on virus assembly. To confirm this hypothesis, the formation of HCoV-OC43 virions in RD cells was examined using transmission electron microscopy (TEM). As shown in Fig. 8A, HCoV-OC43 virions were observed at the enlarged and

fragmented Golgi cisternae, and trafficked in secretory vesicles for egress. The number of virions in cells infected with wild-type virus was higher than with the mutant virus (Fig. 8B). In addition, in HCoV-OC43-WT-infected cells, mature virions showing a dense core were abundant in vesicles (Fig. 8A, upper panels), whereas viral particles in HCoV-OC43-Δns12.9-infected cells exhibiting an aberrant pattern with a translucent central zone (Fig. 8A, lower panels). Quantitative analysis of the virions present in the cytoplasm revealed that the mature virions in cells infected with mutant virus were dramatically decreased compared with cells infected with wild-type virus (Fig. 8C). To confirm these observations, the amount of intracellular mature virions was determined. As expected, a lower titer of intracellular infectious virions was measured in cells infected with HCoV-OC43-Δns12.9 compared with cells infected with HCoV-OC43-WT (Fig. 8D). This decrease in intracellular viral titers of HCoV-OC43-Δns12.9 was consistent with the decreased viral titers observed in the supernatant (Fig. 3). Therefore, these results demonstrate that ns12.9 viroporin facilitates the formation of viral particles and subsequently increases the production of infectious HCoV-OC43 virions.

HCoV-OC43-Δns12.9 is attenuated *in vivo*. To determine the contribution of ns12.9 viroporin to the viral growth *in vivo*, BALB/c mice were infected intranasally with HCoV-OC43-WT or HCoV-OC43-Δns12.9. The infected mice were monitored daily for weight variations and survival. HCoV-OC43-WT-infected mice gained weight normally during the first 3 days, but started to lose weight at 4 dpi. Mice infected with the wild-type virus presented the symptom of less mobility, and all of these mice died at 6 dpi

Journal of Virology

(Fig. 9A and data not shown). However, the HCoV-OC43-Δns12.9-infected mice lost weight more slowly, and exhibited mild disease symptoms and regained weight at 8 dpi with 40% survival (Fig. 9B). The infected mice were sacrificed every 2 dpi to measure the viral titers in brains. As shown in Fig. 9C, the wild-type viral titers were 10- to 100-fold increased compared with mutant viral titers in brains, indicating that HCoV-OC43-Δns12.9 was attenuated in mice.

HCoV-OC43 infection and replication in brains causes lethal encephalitis in mice. To assess the immune response in brains after wild-type and mutant viral infection, the production of key proinflammatory cytokines, such as interleukin (IL)-1β and IL-6, were measured by ELISA. Consistent with the viral titer, significantly increased amounts of proinflammatory cytokines were detected in HCoV-OC43-WT-infected mice compared with HCoV-OC43-Δns12.9-infected mice (Fig. 9D and E), suggesting that HCoV-OC43-WT infection causes more severe inflammatory response in the brain than HCoV-OC43-Δns12.9 infection, which may contribute to the morbidity and mortality.

Collectively, our results indicate that the ns12.9 viroporin is involved in HCoV-OC43 propagation and pathogenesis *in vivo*.

DISCUSSION

Interspersed among the structural genes, CoVs genomes contain accessory genes to encode several accessory proteins that are critical for viral infection (1). An accessory gene located between the S and E structural genes is contained in all CoVs. Thus, this accessory gene may have an important role in CoVs infection. Indeed, down-regulation of this accessory gene by siRNAs (25, 26, 38), deletion of this gene in a cDNA clone using a reverse genetics system (23, 39) or mutation of this gene via cell culture adaptation (40, 41) result in defective viral production and virulence. Previously, we found that this accessory protein 3a in SARS-CoV and ORF4a in HCoV-229E functions as a viroporin to regulate the viral production with an unknown mechanism. In this study, we sought to characterize the functions of this accessory protein ns12.9 in HCoV-OC43 during viral infection. To this end, we engineered an ns12.9 knockout cDNA clone (pBAC-OC43-Δns12.9) with a genetic approach. We demonstrated that the ns12.9 acts as a viroporin in that it has all of the features of viroporins, such as the membrane localization, self-oligomerization and ion channel formation. Furthermore, the absence of ns12.9 led to a lower virus yield *in vitro* and *in vivo*, indicating that the ns12.9 viroporin, although not essential, is important for the production of infectious HCoV-OC43 particles.

The complementation of HCoV-OC43-Δns12.9 in RD cells expressing the ns12.9 accessory protein in *trans* confirmed the importance of ns12.9 on virus replication. Interestingly, this accessory protein from other HCoVs, such as SARS-3a, 229E-ORF4a

and NL63-ORF3, could also rescue the growth of HCoV-OC43-Δns12.9 in *trans* (Fig. 4D). Although there are large variations among these protein sequences (data not shown), they possess similar properties in forming ion channels and regulating viral production (25, 26). Our results strongly suggest that these accessory proteins may exert a conserved viroporin function that is required for virion morphogenesis, which deserves further investigation.

The ion channel activity of viroporins has been reported to associate with the viral production, fitness and pathogenesis (42). In addition to regulate the uncoating stage in the endosome (36), IAV-M2 prevents the excessive acidification of the *trans*-Golgi network (TGN) to induce the correct maturation of viral hemagglutinin glycoprotein (43). The *picornavirus* 2B is present primarily in the Golgi compartments and induces the calcium efflux, which is important for virus release (44-46). In contrast, although it is needed for the late stages of virus life cycle (47, 48), HCV-p7 localizes predominantly to the ER. In the present study, EV71-2B and IAV-M2 viroporins were efficient to complement the ns12.9 knockout virus, while HCV-p7 and the M2Δ29-31 mutant lacking ion conductivity failed to compensate it (Fig. 5). Moreover, the ns12.9 viroporin was found to localize at ERGIC in the infected cells (Fig. 7, middle and lower panels). These results highlight the importance of ion channel activity and ERGIC/Golgi compartments localization of viroporins in HCoV-OC43 infection.

Systematic comparison of HCoV-OC43-WT and HCoV-OC43-Δns12.9 replication revealed that the ns12.9 viroporin is not involved in the early steps of the virus life cycle.

Using electron microscopy, we found that the number of intracellular virions was significantly reduced and that more viral particles exhibited in an aberrant pattern when the ns12.9 protein was deleted (Fig. 8). There are several possibilities that can be responsible for the ns12.9 viroporin promotes the formation of viral particles. First, ns12.9 may function as a structural protein that enhances the production of infectious virus particles. Numerous viroporins are virion-incorporated proteins (36, 49, 50). However, without an effective antibody, we cannot rule out the possibility that the ns12.9 viroporin is a structural protein. Second, ns12.9 may impair the ionic homeostasis of the ERGIC/Golgi compartments, where the CoVs morphogenesis takes place. The ionic equilibration between the ERGIC/Golgi compartments and the cytosol could protect the structural proteins and newly formed virions to promote the virus assembly and maturation (43, 51). Finally, ns12.9 may be involved in membrane scission and promote the budding of progeny virions. Some viroporins have been shown to enhance the membrane permeability, cause membrane depolarization and thus facilitate the membrane scission to trigger the budding process (52-54).

CoVs infection generally exhibits a species-specific property. However, HCoV-OC43 could cross the species barrier to infect the mice and cause encephalitis (55, 56). IL-1β is a main proinflammatory cytokine that initiates pathogenesis of infection (57). Mature IL-1β is cleaved from pro-IL-1β by caspase-1, which is activated by a protein complex termed the inflammasome (58). Inflammasome activation in the central nervous system (CNS) has been studied in various neurological diseases and pathogen infections (59).

Here, we identified robust production of IL-1β in the brain after HCoV-OC43-WT infection (Fig. 9D). This finding may be relevant to the neuropathogenicity of HCoV-OC43. Recently, the viroporins were found to activate the inflammasome in macrophages and dendritic cells (60-63). For HCoV-OC43 infection, ongoing studies are investigating whether the ns12.9 viroporin activate the inflammasome in the microglia, the resident macrophages of the CNS. The type I interferons (IFNs) play an essential role in protection against CoVs infection (64, 65). The MHV 5a, a homologous accessory protein of HCoV-OC43 ns12.9, has been recently reported to be an antagonist of the IFN-induced antiviral action (66). Because HCoV-OC43-Δns12.9 presents propagation reduction and virulence attenuation in mice, the ns12.9 may be a viral factor to antagonize IFN antiviral response during HCoV-OC43 infection, which should be further investigated.

In conclusion, we demonstrated that the ns12.9 accessory protein is a viroporin and influences virion morphogenesis during HCoV-OC43 infection. This study on ns12.9 function provides a potential target for developing antiviral drugs, and contributes to a deeper understanding of the pathogenesis of HCoV-OC43 or other CoVs infections.

ACKNOWLEDGMENTS

We thank Pierre J. Talbot (Laboratory of Neuroimmunovirology, INRS-Institut Armand-Frappier, Laval, Québec, Canada) for providing the pBAC-OC43-WT cDNA clone. We thank Baoqin Xuan (Unit of Herpesvirus and Molecular Virology, Institut Pasteur of Shanghai, Chinese Academy of Sciences, Shanghai, China) for valuable assistance in construction of plasmid pBAC-OC43-Δns12.9. We thank Tianqing Zhang and Fengling Qin (Core Facility of Cell Biology, Institute of Biochemistry and Cell Biology, Chinese Academy of Sciences, Shanghai, China) for their technical assistance in transmission electron microscopy.

This study was supported by the National Science and Technology Major Project (2013ZX10004-101-005, 2012ZX10002-007-003 and 2013ZX10004-003-003).

REFERENCES

1. **Masters P.** 2006. The Molecular Biology of Coronaviruses. Advances in Virus Research **66:**193-292.
2. **Adams MJ, Carstens EB.** 2012. Ratification vote on taxonomic proposals to the International Committee on Taxonomy of Viruses (2012). Archives of Virology **157:**1411-1422.
3. **McIntosh K, Becker WB, Chanock RM.** 1967. Growth in suckling-mouse brain of "IBV-like" viruses from patients with upper respiratory tract disease. Proc Natl Acad Sci U S A **58:**2268-2273.
4. **Myint SH.** 1994. Human Coronaviruses - a Brief Review. Reviews in Medical Virology **4:**35-46.
5. **Arbour N, Day R, Newcombe J, Talbot PJ.** 2000. Neuroinvasion by human respiratory coronaviruses. J Virol **74:**8913-8921.
6. **Arbour N, Cote G, Lachance C, Tardieu M, Cashman NR, Talbot PJ.** 1999. Acute and persistent infection of human neural cell lines by human coronavirus OC43. J Virol **73:**3338-3350.
7. **Stewart JN, Mounir S, Talbot PJ.** 1992. Human coronavirus gene expression in the brains of multiple sclerosis patients. Virology **191:**502-505.
8. **Ziebuhr J, Snijder EJ, Gorbalenya AE.** 2000. Virus-encoded proteinases and proteolytic processing in the Nidovirales. J Gen Virol **81:**853-879.
9. **Vlasak R, Luytjes W, Spaan W, Palese P.** 1988. Human and bovine coronaviruses

recognize sialic acid-containing receptors similar to those of influenza C viruses. Proc Natl Acad Sci U S A **85:**4526-4529.

10. **Li W, Moore MJ, Vasilieva N, Sui J, Wong SK, Berne MA, Somasundaran M, Sullivan JL, Luzuriaga K, Greenough TC, Choe H, Farzan M.** 2003. Angiotensin-converting enzyme 2 is a functional receptor for the SARS coronavirus. Nature **426:**450-454.
11. **Raj VS, Mou H, Smits SL, Dekkers DH, Muller MA, Dijkman R, Muth D, Demmers JA, Zaki A, Fouchier RA, Thiel V, Drosten C, Rottier PJ, Osterhaus AD, Bosch BJ, Haagmans BL.** 2013. Dipeptidyl peptidase 4 is a functional receptor for the emerging human coronavirus-EMC. Nature **495:**251-254.
12. **Yeager CL, Ashmun RA, Williams RK, Cardellichio CB, Shapiro LH, Look AT, Holmes KV.** 1992. Human Aminopeptidase N Is a Receptor for Human Coronavirus 229E. Nature **357:**420-422.
13. **Vennema H, Godeke GJ, Rossen JW, Voorhout WF, Horzinek MC, Opstelten DJ, Rottier PJ.** 1996. Nucleocapsid-independent assembly of coronavirus-like particles by co-expression of viral envelope protein genes. EMBO J **15:**2020-2028.
14. **Huang Y, Yang ZY, Kong WP, Nabel GJ.** 2004. Generation of synthetic severe acute respiratory syndrome coronavirus pseudoparticles: implications for assembly and vaccine production. J Virol **78:**12557-12565.
15. **Corse E, Machamer CE.** 2000. Infectious bronchitis virus E protein is targeted to the Golgi complex and directs release of virus-like particles. Journal of Virology

74:4319-4326.

16. **Schultze B, Wahn K, Klenk HD, Herrler G.** 1991. Isolated HE-protein from hemagglutinating encephalomyelitis virus and bovine coronavirus has receptor-destroying and receptor-binding activity. Virology **180:**221-228.
17. **Desforges M, Desjardins J, Zhang C, Talbot PJ.** 2013. The acetyl-esterase activity of the hemagglutinin-esterase protein of human coronavirus OC43 strongly enhances the production of infectious virus. J Virol **87:**3097-3107.
18. **Ortego J, Sola I, Almazan F, Ceriani JE, Riquelme C, Balasch M, Plana J, Enjuanes L.** 2003. Transmissible gastroenteritis coronavirus gene 7 is not essential but influences in vivo virus replication and virulence. Virology **308:**13-22.
19. **Haijema BJ, Volders H, Rottier PJM.** 2004. Live, attenuated coronavirus vaccines through the directed deletion of group-specific genes provide protection against feline infectious peritonitis. Journal of Virology **78:**3863-3871.
20. **Schaecher SR, Touchette E, Schriewer J, Buller RM, Pekosz A.** 2007. Severe acute respiratory syndrome coronavirus gene 7 products contribute to virus-induced apoptosis. J Virol **81:**11054-11068.
21. **Kopecky-Bromberg SA, Martinez-Sobrido L, Frieman M, Baric RA, Palese P.** 2007. Severe acute respiratory syndrome coronavirus open reading frame (ORF) 3b, ORF 6, and nucleocapsid proteins function as interferon antagonists. J Virol **81:**548-557.
22. **de Haan CAM, Masters PS, Shen XL, Weiss S, Rottier PJM.** 2002. The

group-specific murine coronavirus genes are not essential, but their deletion, by reverse genetics, is attenuating in the natural host. Virology **296:**177-189.

23. **Yount B, Roberts RS, Sims AC, Deming D, Frieman MB, Sparks J, Denison MR, Davis N, Baric RS.** 2005. Severe acute respiratory syndrome coronavirus group-specific open reading frames encode nonessential functions for replication in cell cultures and mice. J Virol **79:**14909-14922.

24. **Youn S, Leibowitz JL, Collisson EW.** 2005. In vitro assembled, recombinant infectious bronchitis viruses demonstrate that the 5a open reading frame is not essential for replication. Virology **332:**206-215.

25. **Zhang RH, Wang K, Lv W, Yu WJ, Xie SQ, Xu K, Schwarz W, Xiong SD, Sun B.** 2014. The ORF4a protein of human coronavirus 229E functions as a viroporin that regulates viral production. Biochimica et Biophysica Acta (BBA) - Biomembranes **1838:**1088-1095.

26. **Lu W, Zheng BJ, Xu K, Schwarz W, Du L, Wong CK, Chen J, Duan S, Deubel V, Sun B.** 2006. Severe acute respiratory syndrome-associated coronavirus 3a protein forms an ion channel and modulates virus release. Proc Natl Acad Sci U S A **103:**12540-12545.

27. **Nieva JL, Madan V, Carrasco L.** 2012. Viroporins: structure and biological functions. Nat Rev Microbiol **10:**563-574.

28. **Mounir S, Labonte P, Talbot PJ.** 1993. Characterization of the nonstructural and spike proteins of the human respiratory coronavirus OC43: comparison with bovine

enteric coronavirus. Adv Exp Med Biol **342:**61-67.

29. **Qian Z, Xuan B, Gualberto N, Yu D.** 2011. The human cytomegalovirus protein pUL38 suppresses endoplasmic reticulum stress-mediated cell death independently of its ability to induce mTORC1 activation. J Virol **85:**9103-9113.
30. **Lambert F, Jacomy H, Marceau G, Talbot PJ.** 2008. Titration of human coronaviruses, HcoV-229E and HCoV-OC43, by an indirect immunoperoxidase assay. Methods Mol Biol **454:**93-102.
31. **St-Jean JR, Desforges M, Almazan F, Jacomy H, Enjuanes L, Talbot PJ.** 2006. Recovery of a Neurovirulent Human Coronavirus OC43 from an Infectious cDNA Clone. Journal of Virology **80:**3670-3674.
32. **St-Jean JR, Jacomy H, Desforges M, Vabret A, Freymuth F, Talbot PJ.** 2004. Human respiratory coronavirus OC43: genetic stability and neuroinvasion. J Virol **78:**8824-8834.
33. **Kyte J, Doolittle RF.** 1982. A simple method for displaying the hydropathic character of a protein. J Mol Biol **157:**105-132.
34. **Wang K, Xie SQ, Sun B.** 2011. Viral proteins function as ion channels. Biochimica et Biophysica Acta (BBA) - Biomembranes **1808:**510-515.
35. **Gonzalez ME, Carrasco L.** 2003. Viroporins. FEBS Letters **552:**28-34.
36. **Pinto LH, Holsinger LJ, Lamb RA.** 1992. Influenza Virus M2 Protein Has Ion Channel Activity. Cell **69:**517-528.
37. **Watanabe T, Watanabe S, Ito H, Kida H, Kawaoka Y.** 2001. Influenza a virus can

undergo multiple cycles of replication without M2 ion channel activity. Journal of Virology **75:**5656-5662.

38. **Åkerström S, Mirazimi A, Tan Y-J.** 2007. Inhibition of SARS-CoV replication cycle by small interference RNAs silencing specific SARS proteins, 7a/7b, 3a/3b and S. Antiviral Research **73:**219-227.

39. **Donaldson EF, Yount B, Sims AC, Burkett S, Pickles RJ, Baric RS.** 2008. Systematic Assembly of a Full-Length Infectious Clone of Human Coronavirus NL63. Journal of Virology **82:**11948-11957.

40. **Woods RD.** 2001. Efficacy of a transmissible gastroenteritis coronavirus with an altered ORF-3 gene. Can J Vet Res **65:**28-32.

41. **Song DS, Yang JS, Oh JS, Han JH, Park BK.** 2003. Differentiation of a Vero cell adapted porcine epidemic diarrhea virus from Korean field strains by restriction fragment length polymorphism analysis of ORF 3. Vaccine **21:**1833-1842.

42. **Nieto-Torres JL, Verdia-Baguena C, Castano-Rodriguez C, Aguilella VM, Enjuanes L.** 2015. Relevance of Viroporin Ion Channel Activity on Viral Replication and Pathogenesis. Viruses **7:**3552-3573.

43. **Ciampor F, Bayley PM, Nermut MV, Hirst EMA, Sugrue RJ, Hay AJ.** 1992. Evidence that the amantadine-induced, M2-mediated conversion of influenza A virus hemagglutinin to the low PH conformation occurs in an acidic transgolgi compartment. Virology **188:**14-24.

44. **Campanella M, de Jong AS, Lanke KWH, Melchers WJG, Willems PHGM,**

673 **Pinton P, Rizzuto R, van Kuppeveld FJM.** 2004. The coxsackievirus 2B protein
674 suppresses apoptotic host cell responses by manipulating intracellular Ca2+
675 homeostasis. Journal of Biological Chemistry **279:**18440-18450.
676 45. **de Jong AS, de Mattia F, Van Dommelen MM, Lanke K, Melchers WJG,**
677 **Willems PHGM, van Kuppeveld FJM.** 2008. Functional analysis of picornavirus
678 2B proteins: effects on calcium homeostasis and intracellular protein trafficking.
679 Journal of Virology **82:**3782-3790.
680 46. **vanKuppeveld FJM, Hoenderop JGJ, Smeets RLL, Willems PHGM, Dijkman**
681 **HBPM, Galama JMD, Melchers WJG.** 1997. Coxsackievirus protein 2B modifies
682 endoplasmic reticulum membrane and plasma membrane permeability and facilitates
683 virus release. Embo Journal **16:**3519-3532.
684 47. **Steinmann E, Pietschmann T.** 2010. Hepatitis C Virus P7—A Viroporin Crucial for
685 Virus Assembly and an Emerging Target for Antiviral Therapy. Viruses **2:**2078-2095.
686 48. **Steinmann E, Penin F, Kallis S, Patel AH, Bartenschlager R, Pietschmann T.**
687 2007. Hepatitis C virus p7 protein is crucial for assembly and release of infectious
688 virions. PLoS Pathogens **3:**e103.
689 49. **Wilson L, McKinlay C, Gage P, Ewart G.** 2004. SARS coronavirus E protein forms
690 cation-selective ion channels. Virology **330:**322-331.
691 50. **Ito N, Mossel EC, Narayanan K, Popov VL, Huang C, Inoue T, Peters CJ,**
692 **Makino S.** 2005. Severe acute respiratory syndrome coronavirus 3a protein is a viral
693 structural protein. Journal of Virology **79:**3182-3186.

694 51. **Michelangeli F, Liprandi F, Chemello ME, Ciarlet M, Ruiz MC.** 1995. Selective
695 depletion of stored calcium by thapsigargin blocks rotavirus maturation but not the
696 cytopathic effect. J Virol **69:**3838-3847.
697 52. **Hsu K, Han J, Shinlapawittayatorn K, Deschenes I, Marban E.** 2010. Membrane
698 potential depolarization as a triggering mechanism for Vpu-mediated HIV-1 release.
699 Biophysical Journal **99:**1718-1725.
700 53. **Huang DTN, Chi NW, Chen SC, Lee TY, Hsu K.** 2011. Background K(2P)
701 channels KCNK3/9/15 limit the budding of cell membrane-derived vesicles. Cell
702 Biochemistry and Biophysics **61:**585-594.
703 54. **DeDiego ML, Alvarez E, Almazan F, Rejas MT, Lamirande E, Roberts A, Shieh**
704 **WJ, Zaki SR, Subbarao K, Enjuanes L.** 2007. A severe acute respiratory syndrome
705 coronavirus that lacks the E gene is attenuated in vitro and in vivo. Journal of
706 Virology **81:**1701-1713.
707 55. **Jacomy H, Talbot PJ.** 2003. Vacuolating encephalitis in mice infected by human
708 coronavirus OC43. Virology **315:**20-33.
709 56. **Butler N, Pewe L, Trandem K, Perlman S.** 2006. Murine encephalitis caused by
710 HCoV-OC43, a human coronavirus with broad species specificity, is partly
711 immune-mediated. Virology **347:**410-421.
712 57. **Tisoncik JR, Korth MJ, Simmons CP, Farrar J, Martin TR, Katze MG.** 2012.
713 Into the Eye of the Cytokine Storm. Microbiology and Molecular Biology Reviews
714 **76:**16-32.

58. **Martinon F, Burns K, Tschopp J.** 2002. The inflammasome: a molecular platform triggering activation of inflammatory caspases and processing of proIL-beta. Mol Cell **10:**417-426.

59. **Chakraborty S, Kaushik DK, Gupta M, Basu A.** 2010. Inflammasome signaling at the heart of central nervous system pathology. Journal of Neuroscience Research **88:**1615-1631.

60. **Ichinohe T, Pang IK, Iwasaki A.** 2010. Influenza virus activates inflammasomes via its intracellular M2 ion channel. Nature Immunology **11:**404-410.

61. **Nieto-Torres JL, DeDiego ML, Verdiá-Báguena C, Jimenez-Guardeño JM, Regla-Nava JA, Fernandez-Delgado R, Castaño-Rodriguez C, Alcaraz A, Torres J, Aguilella VM, Enjuanes L.** 2014. Severe Acute Respiratory Syndrome Coronavirus Envelope Protein Ion Channel Activity Promotes Virus Fitness and Pathogenesis. PLoS Pathogens **10:**e1004077.

62. **Ito M, Yanagi Y, Ichinohe T.** 2012. Encephalomyocarditis virus viroporin 2B activates NLRP3 inflammasome. PLoS Pathog **8:**e1002857.

63. **Triantafilou K, Kar S, Vakakis E, Kotecha S, Triantafilou M.** 2013. Human respiratory syncytial virus viroporin SH: a viral recognition pathway used by the host to signal inflammasome activation. Thorax **68:**66-75.

64. **Cervantes-Barragan L, Zust R, Weber F, Spiegel M, Lang KS, Akira S, Thiel V, Ludewig B.** 2007. Control of coronavirus infection through plasmacytoid dendritic-cell-derived type I interferon. Blood **109:**1131-1137.

736 65. **Ireland DDC, Stohlman SA, Hinton DR, Atkinson R, Bergmann CC.** 2008. Type
737 I interferons are essential in controlling neurotropic coronavirus infection
738 irrespective of functional CD8 T cells. Journal of Virology **82:**300-310.
739 66. **Koetzner CA, Kuo LL, Goebel SJ, Dean AB, Parker MM, Masters PS.** 2010.
740 Accessory Protein 5a Is a Major Antagonist of the Antiviral Action of Interferon
741 against Murine Coronavirus. Journal of Virology **84:**8262-8274.
742
743

Figure legend

FIG 1 The ns12.9 accessory protein of HCoV-OC43 acts as a viroporin. (A) Kyte-Doolittle hydropathy plot of ns12.9 protein. The hydropathy plot was drawn with a window size of 19 using the Kyte-Doolittle method of hydrophilicity calculation. (B) Indirect immunofluorescence analysis of cell membrane expression of ns12.9 in RD cells transfected with pCAGGS-ns12.9-HA or empty vectors. Cells were fixed, non-permeabilized and subjected to incubation with anti-HA monoclonal antibody, followed by staining with Alexa Fluor 488-conjugated goat anti-mouse antibody (green). Nuclei were stained with DAPI (blue). Bars represent 15 μm. (C) Flow cytometry analysis of cell membrane expression of ns12.9 in 293T cells transfected with pCAGGS-ns12.9-HA or empty vectors. Cells were non-permeabilized and stained with anti-HA monoclonal antibody, followed by Alexa Fluor 488-conjugated goat anti-mouse antibody. (D) Reciprocal coimmunoprecipitation assay of ns12.9-HA and ns12.9-Flag in 293T cells. Cells were transfected with pCAGGS-ns12.9-HA or pCAGGS-ns12.9-Flag vectors and lysed at 24 hours post-transfection. Cell lysates were subjected to immunoprecipitation with anti-HA agarose or ANTI-FLAG M2 affinity gel. The immunoprecipitated proteins were determined by western blotting using polyclonal anti-Flag and anti-HA antibody. (E) Oligomerization of the ns12.9-HA protein. The HA immunoprecipitates from cells transfected with pCAGGS-ns12.9-HA or empty vectors were analyzed by western blotting with polyclonal anti-HA antibody. The monomer and oligomers were indicated with arrowhead and arrows, respectively. Representative

765 current traces (F) and *I*/*V* relationship of the currents (G) in ns12.9-expressing and control
766 oocytes. During the current recording, the oocytes were bathed in the ORi solution, and
767 the standard voltage-clamp protocol consisted of rectangular voltage pulses from -150 to
768 +30 mV in 10-mV increments applied from a holding voltage of -60 mV. Data represent
769 the mean ± SD (n = 5). (H) Complementation of the potassium uptake-deficient yeast.
770 The yeasts transformed with empty or ns12.9-expressing vector were grown in parallel on
771 plates supplemented with 100 mM KCl or 0.2 mM KCl. Plates were kept at 30 °C for 3-4
772 days.
773
774 **FIG 2** Rescue of HCoV-OC43-Δns12.9 from the recombinant mutant
775 pBAC-OC43-Δns12.9 cDNA clone. (A) Schematic representation of the wild-type
776 (pBAC-OC43-WT) and ns12.9 knockout cDNA (pBAC-OC43-Δns12.9) clone. To
777 construct the pBAC-OC43-Δns12.9 clone, the G12A nucleotide (underlined) was
778 changed to a stop codon at Trp4, and an 82-nt segment was inserted behind the mutant
779 stop codon to avoid the possibility of genetic reversion. The EcoRI restriction sites are
780 denoted by arrows. (B) EcoRI restriction digestion analysis of recombinant
781 pBAC-OC43-WT and pBAC-OC43-Δns12.9. The pBAC-OC43-WT plasmid was cleaved
782 into 7 fragments (9802, 9104, 7632, 4916, 3438, 2553 and 1427 bp), whereas the
783 pBAC-OC43-Δns12.9 plasmid was cleaved into 8 fragments with an additional EcoRI
784 restriction site at the 82-nt inserted segment that led to the 9802-bp fragment being recut
785 into 5782- and 4102-bp fragments. The arrowheads indicate different fragments between

786 the pBAC-OC43-WT and pBAC-OC43-Δns12.9 plasmid. (C) Viral RNA was extracted
787 from the supernatants of the infected RD cells and used to amplify the ns12.9 gene. (D)
788 Indirect immunofluorescence analysis of HCoV-OC43 N proteins in RD cells. Cells were
789 labeled with the OC43-N mouse monoclonal antibody, and the Alexa Fluor
790 488-conjugated goat anti-mouse antibody (green) was used as the secondary antibody.
791 Bars represent 40 μm.
792
793 **FIG 3** The ns12.9 accessory protein is important for HCoV-OC43 replication *in vitro*.
794 Growth kinetic analysis of HCoV-OC43-Δns12.9 in BHK-21 (A) and RD cells (B). Cells
795 were infected with HCoV-OC43-WT or HCoV-OC43-Δns12.9 at a MOI of 0.1, and
796 supernatants were collected at the indicated times to determine the viral titers using IPA.
797 Data represent the mean ± SD and were generated from three independent experiments.
798
799 **FIG 4** The complementation of HCoV-OC43-Δns12.9 infection in RD cells expressing
800 ns12.9 and this accessory protein from other CoVs. (A) Transient expression of
801 exogenous ns12.9. Cells were transfected with a vector expressing ns12.9-HA or a control
802 vector using Lipofectamine LTX (Life Technologies). The expression levels of
803 ns12.9-HA was determined at 48 hours post-transfection by western blotting. (B)
804 Expression of ns12.9 in RD cells enhances the viral production. After 24 hours
805 post-transfection, RD cells were infected with HCoV-OC43-WT or HCoV-OC43-Δns12.9
806 at a MOI of 1. Cell supernatants were collected at 72 hpi, and the viral titers were

807 determined by IPA. (C) Transient expression of ns12.9 and this accessory protein from
808 other CoVs. The expression levels of OC43-ns12.9, SARS-3a, NL63-ORF3 and
809 229E-ORF4a were determined at 48 hours post-transfection by western blotting. Asterisk
810 indicates a putative truncated variant of full-length 229E-ORF4a. (D) Expression of
811 accessory proteins compensates the production of HCoV-OC43-Δns12.9. After 24 hours
812 post-transfection, RD cells were infected with HCoV-OC43-Δns12.9 at a MOI of 1, and
813 the cell supernatants were collected to determine the viral titers at 72 hpi. Data represent
814 the mean ± SD and were generated from three independent experiments. Statistical
815 significance: *, $P < 0.05$; **, $P < 0.01$.
816
817 **FIG 5** The complementation of HCoV-OC43-Δns12.9 infection in RD cells expressing
818 viroporins. (A) Transient expression of ns12.9 and other viroporins. The expression levels
819 of OC43-ns12.9, IAV-M2, EV71-2B and HCV-p7 were determined at 48 hours
820 post-transfection by western blotting. (B) The M2 and 2B viroporins compensate the
821 production of HCoV-OC43-Δns12.9. After 24 hours post-transfection, RD cells were
822 infected with HCoV-OC43-Δns12.9 at a MOI of 1. Cell supernatants were collected at 72
823 hpi, and the viral titers were determined by IPA. (C) Transient expression of M2 and
824 M2Δ29-31 mutant. The expression levels of M2 and M2Δ29-31 mutant were determined
825 at 48 hours post-transfection by western blotting. (D) The M2Δ29-31 mutant does not
826 compensate the production of HCoV-OC43-Δns12.9. After 24 hours post-transfection,
827 RD cells were infected with HCoV-OC43-Δns12.9 at a MOI of 1. Cell supernatants were

collected at 72 hpi, and the viral titers were determined by IPA. Data represent the mean ± SD and were generated from three independent experiments. Statistical significance: ns, not significant; *, $P < 0.05$; **, $P < 0.01$.

FIG 6 The ns12.9 accessory protein does not affect the early steps of HCoV-OC43 infection and protein expression. (A) Knockout of ns12.9 gene does not impair the entry process. RD cells were infected with HCoV-OC43-WT or HCoV-OC43-Δns12.9 at a MOI of 1, and fixed at 0.5 and 1.5 hpi. Cells were stained with an OC43-N mouse monoclonal antibody, and the Alexa Fluor 488-conjugated goat anti-mouse antibody was used as the secondary antibody. The stained cells were analyzed by flow cytometry. The results are representative of three independent experiments. (B) Knockout of ns12.9 gene does not impair viral RNA replication. Cells were infected with HCoV-OC43-WT or HCoV-OC43-Δns12.9 at a MOI of 1, and total RNA was extracted at 2, 4, 6 and 8 hpi. Viral RNA levels were analyzed by qRT-PCR with the OC43-RT primers. (C) Knockout of ns12.9 gene does not impair sgmRNA synthesis. Total RNA was extracted from the infected cells at 8 hpi, and HCoV-OC43 sgmRNA levels were analyzed by qRT-PCR using the specific primers presented in Table 1. Data represent the mean ± SD and were generated from three independent experiments. Statistical significance: **, $P < 0.01$. (D) Knockout of ns12.9 gene does not impair OC43-N protein expression. Cell lysates were collected at 12, 18 and 24 hpi, and the expression levels of OC43-N protein were determined by western blotting. The bands were analyzed and the fold changes of N

849 protein at indicated times were calculated considering the wild- type infected cells as 1
850 with actin as internal control.
851
852 **FIG 7** Subcellular localization of ns12.9 during HCoV-OC43 infection. RD cells were
853 infected with HCoV-OC43-WT or HCoV-OC43-Δns12.9 at a MOI of 1. At 24 hours
854 post-infection, cells were transfected with pCAGGS-ns12.9-HA. Cells were fixed and
855 examined by confocal microscopy analysis at 24 hours post-transfection. The ns12.9 was
856 stained with anti-HA monoclonal antibody and visualized with Alexa Fluor
857 488-conjugated goat anti-mouse antibody (green). ERGIC was stained with ERGIC53
858 antibody (H-245) and visualized with Cy3-conjugated goat anti-rabbit antibody (red).
859 Nuclei were stained with DAPI (blue). Bars represent 20 μm.
860
861 **FIG 8** Electron microscopy analysis of HCoV-OC43 virions morphogenesis. (A)
862 Transmission electron micrographs of virions in the infected RD cells. Cells were
863 infected with HCoV-OC43-WT or HCoV-OC43-Δns12.9 at a MOI of 1, fixed at 24 hpi
864 and processed for transmission electron microscopy. The virions were found in the Golgi
865 complex (circles) and secretory vesicles (asterisks). The thick arrows indicate the mature
866 virions, and the thin arrows indicate the aberrant virions. Quantification of total numbers
867 of virions (B) and the mature or aberrant virions (C). The virions in
868 HCoV-OC43-WT-infected cells (n = 9) or HCoV-OC43-Δns12.9 cells (n = 10) were
869 counted, and data were plotted as the mean ± SD. Statistical significance: ***, $P < 0.001$.

(D) Titration of the intracellular infectious virions. RD cells were infected with HCoV-OC43-WT or HCoV-OC43-Δns12.9 at a MOI of 1. Cells were collected at 24 hpi and disrupted by three cycles of freeze-thawing in dry ice and a 37°C water bath. The intracellular infectious viruses were determined by IPA. Data represent the mean ± SD and were generated from three independent experiments. Statistical significance: **, $P < 0.01$.

FIG 9 HCoV-OC43-Δns12.9 is attenuated in growth and virulence *in vivo*. Mice were intranasally inoculated with HCoV-OC43-WT or HCoV-OC43-Δns12.9. Infected mice were monitored daily for weight variations and sacrificed every 2 dpi to measure the viral titers or proinflammatory cytokines in brains. The weight variations (A) and survival curves (B) after infection are presented for each group. (C) The Viral titers in the brains of the infected mice at the indicated times were determined by IPA. Statistical significance: *, $P < 0.05$; **, $P < 0.01$. The production of IL-1β (D) and IL-6 (E) proinflammatory cytokines at the indicated times was measured by ELISA. Data represent the mean ± SD from samples of 4 mice. Statistical significance: *, $P < 0.05$.

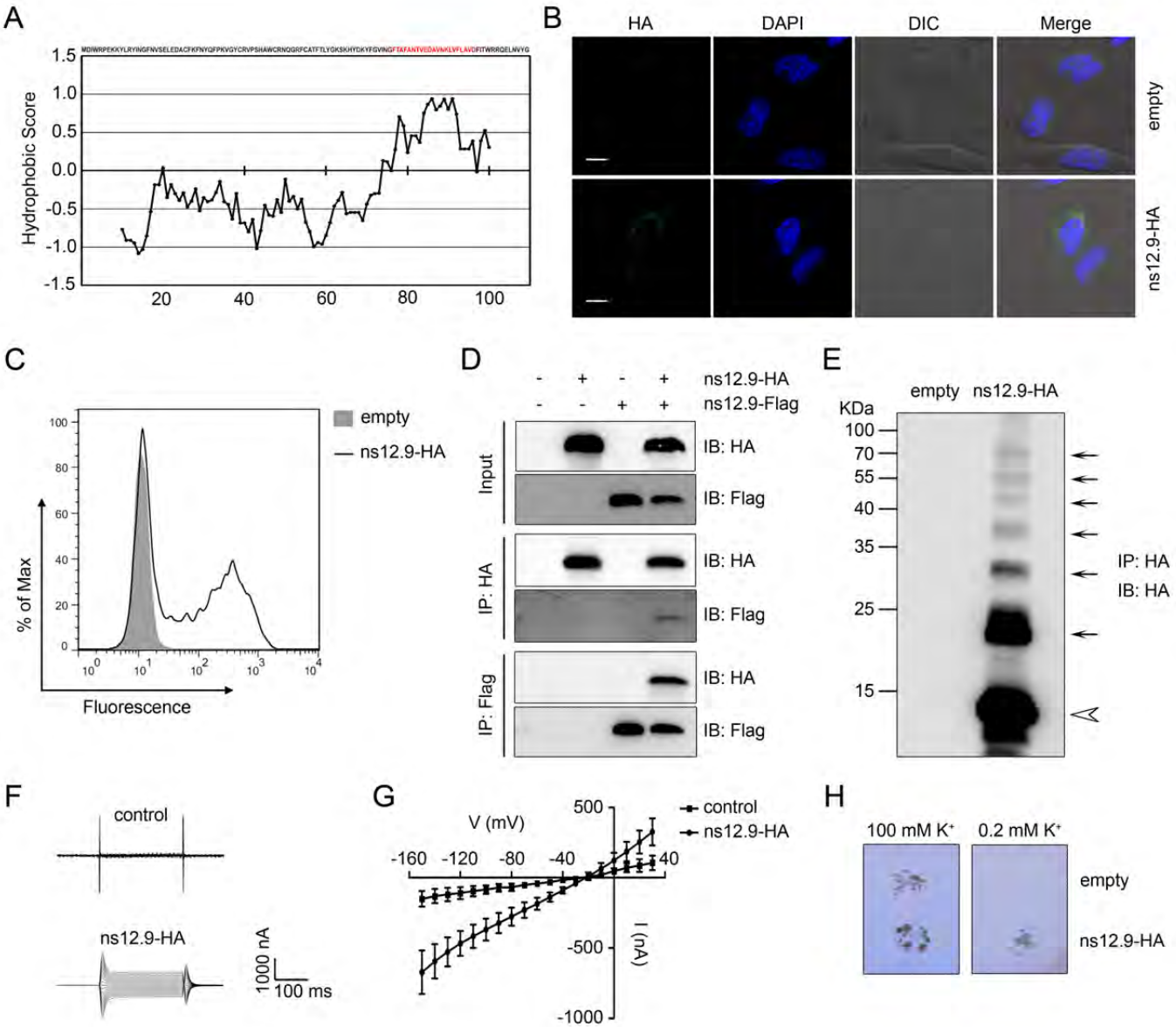

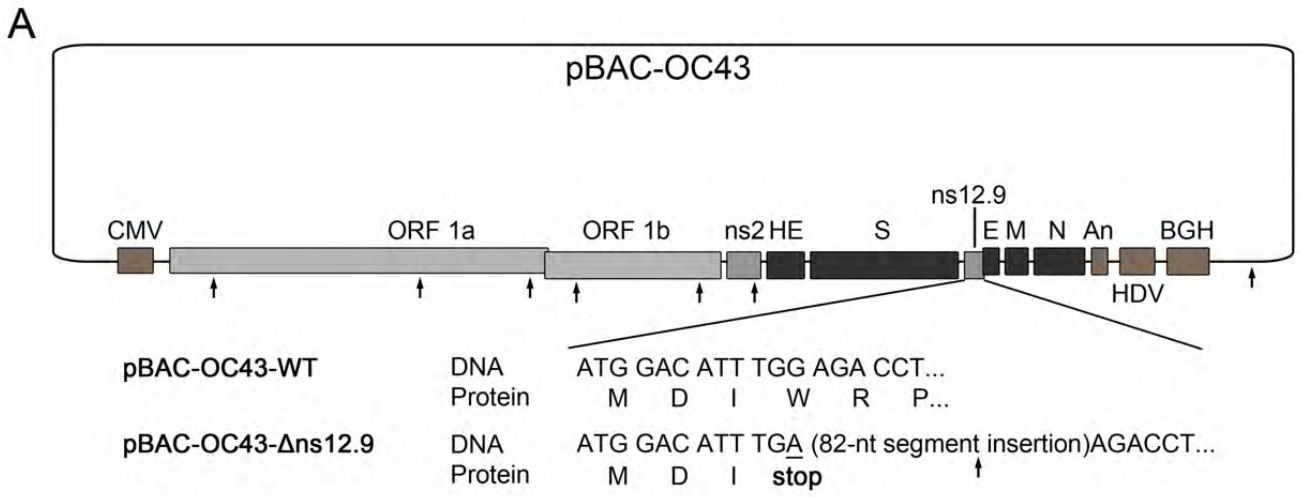

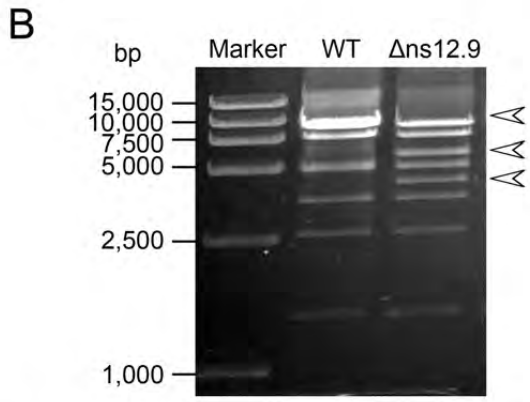

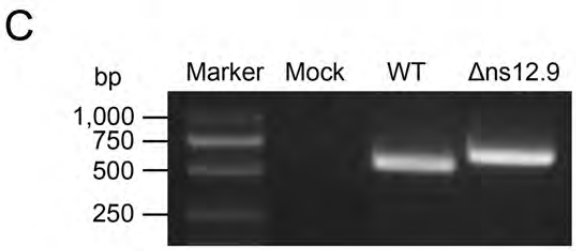

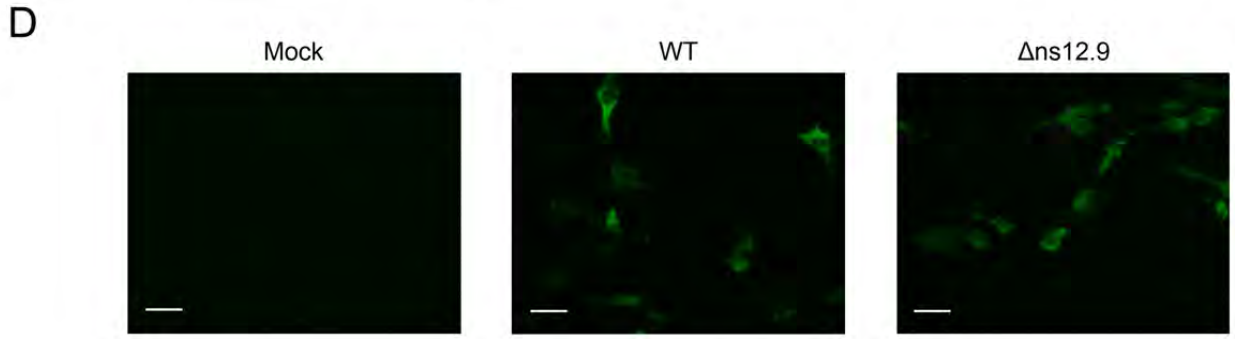

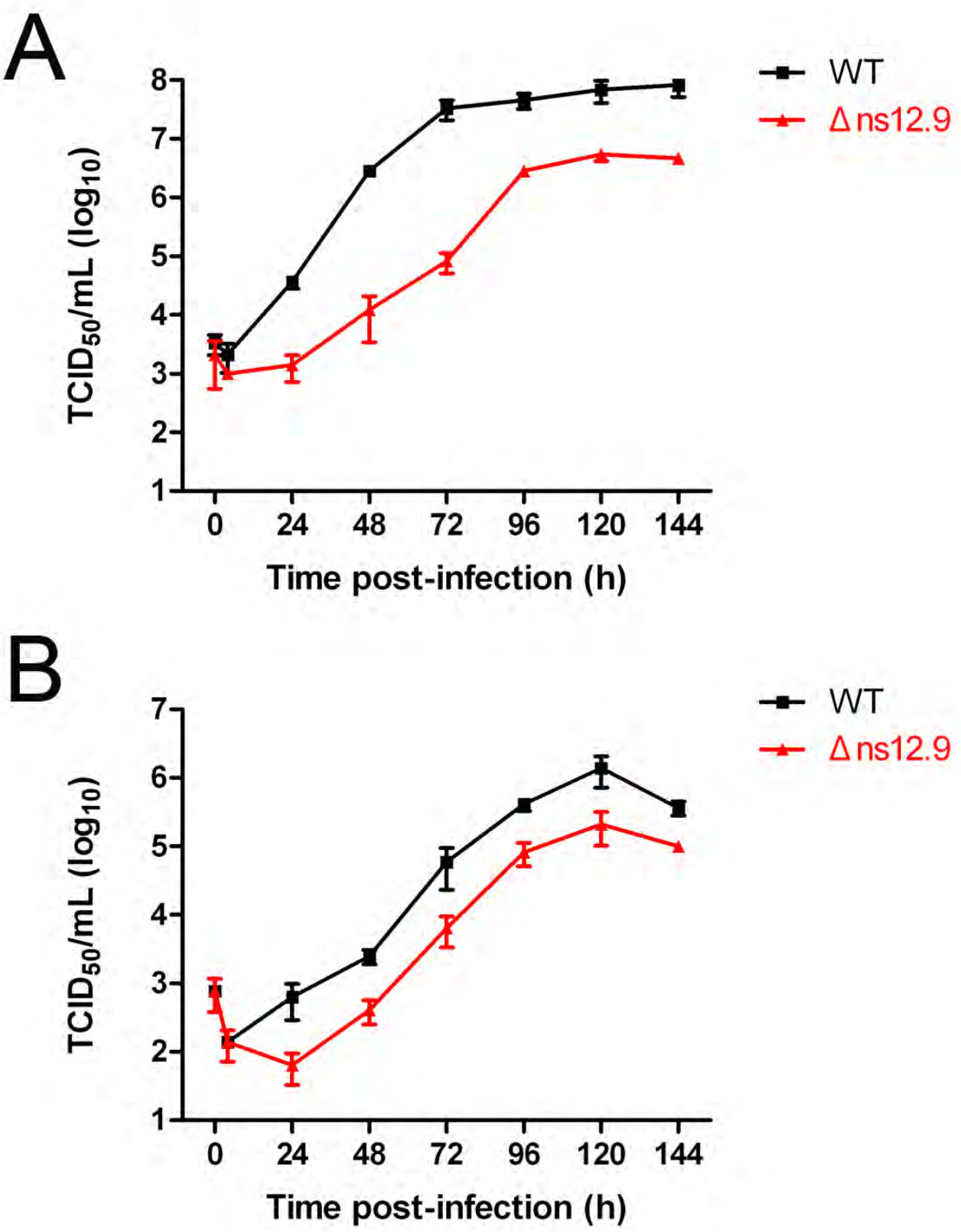

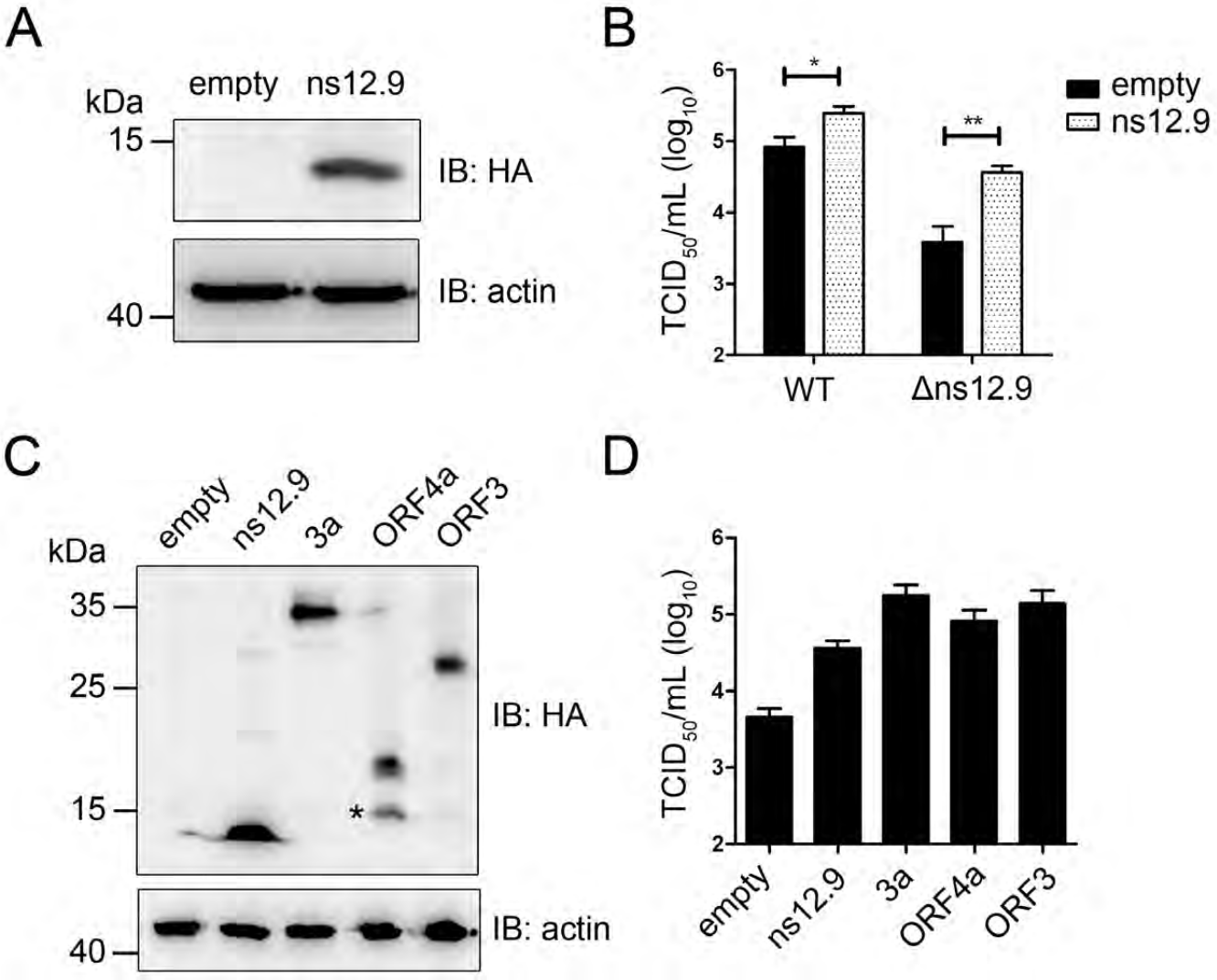

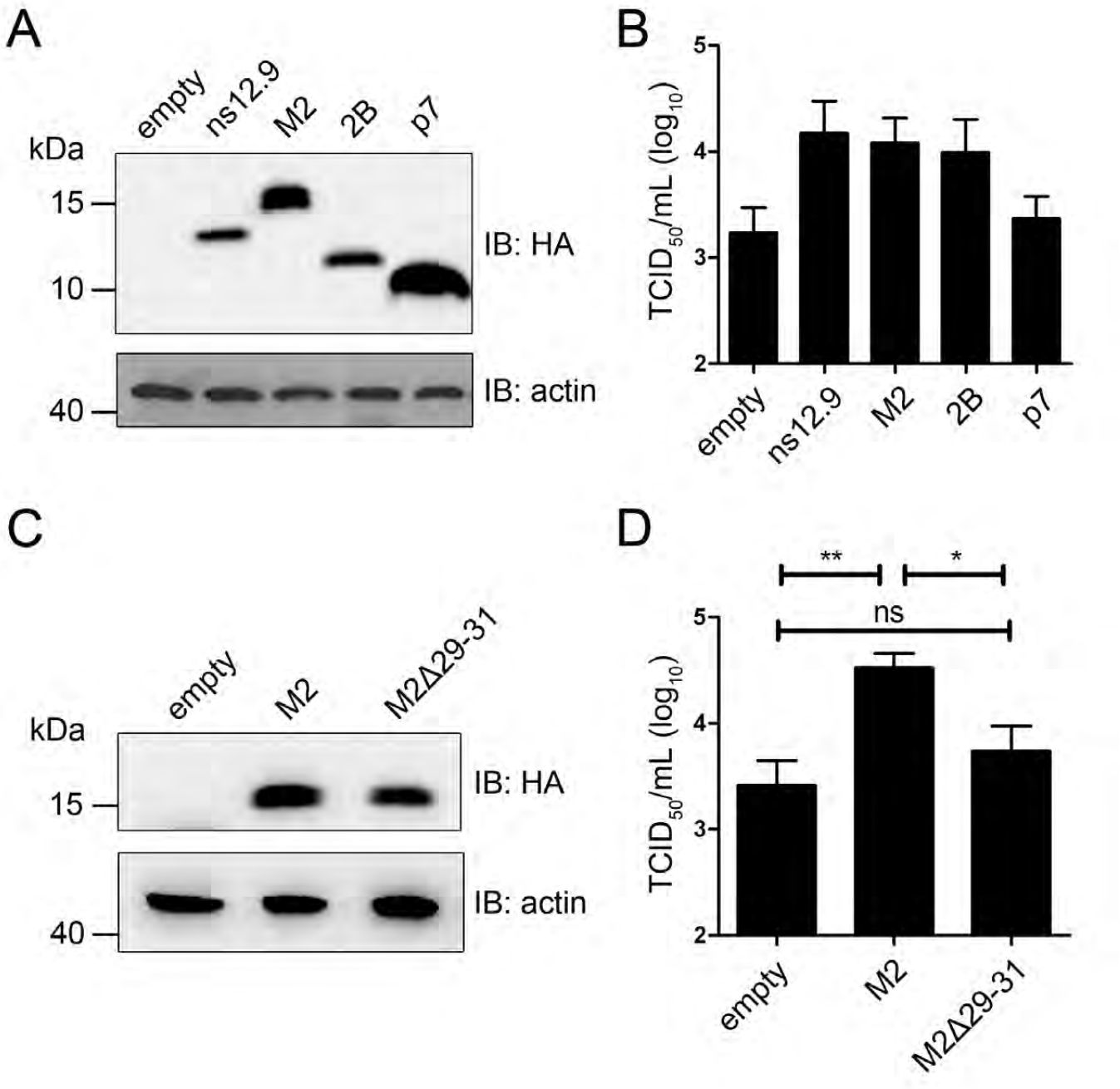

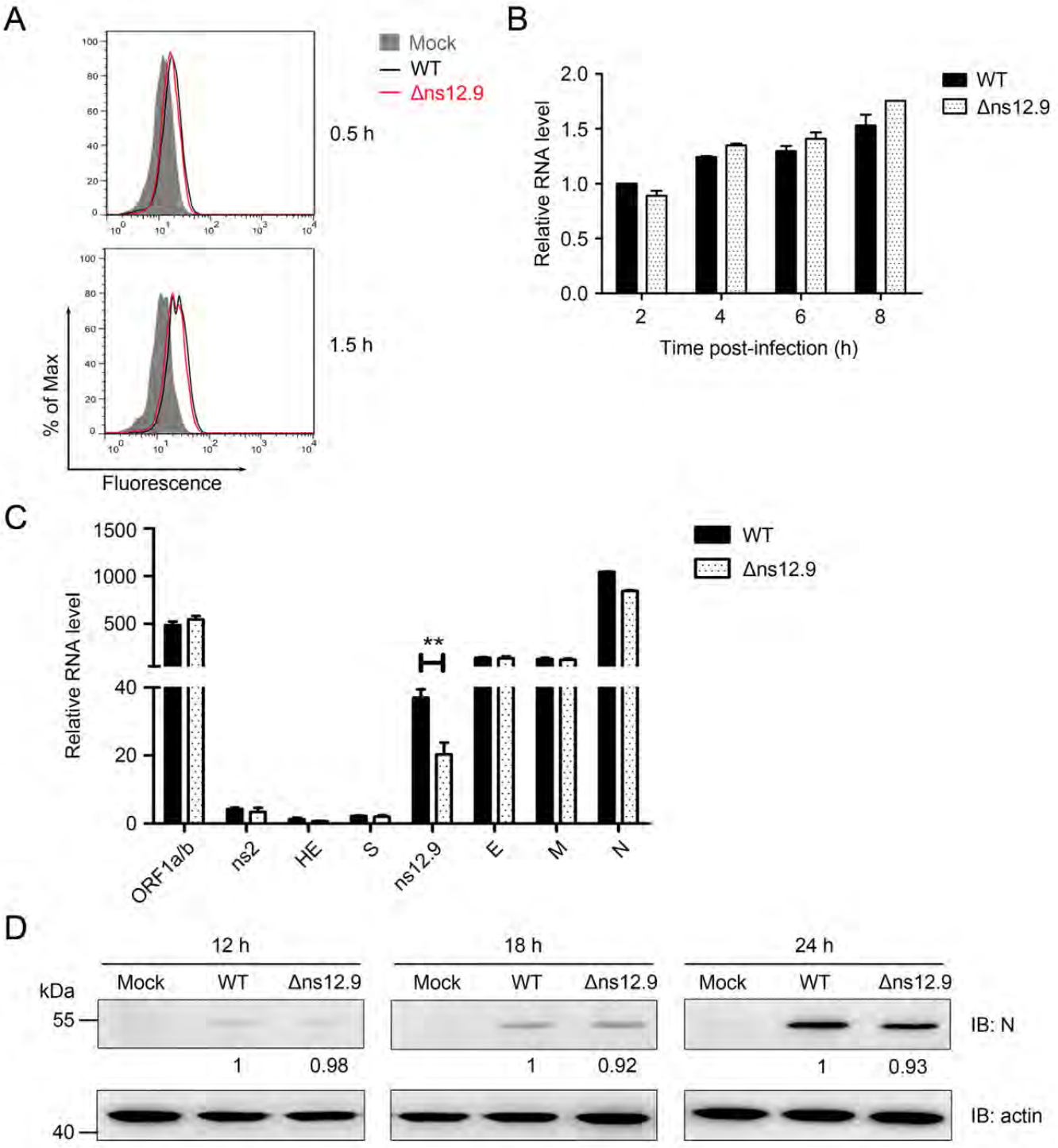

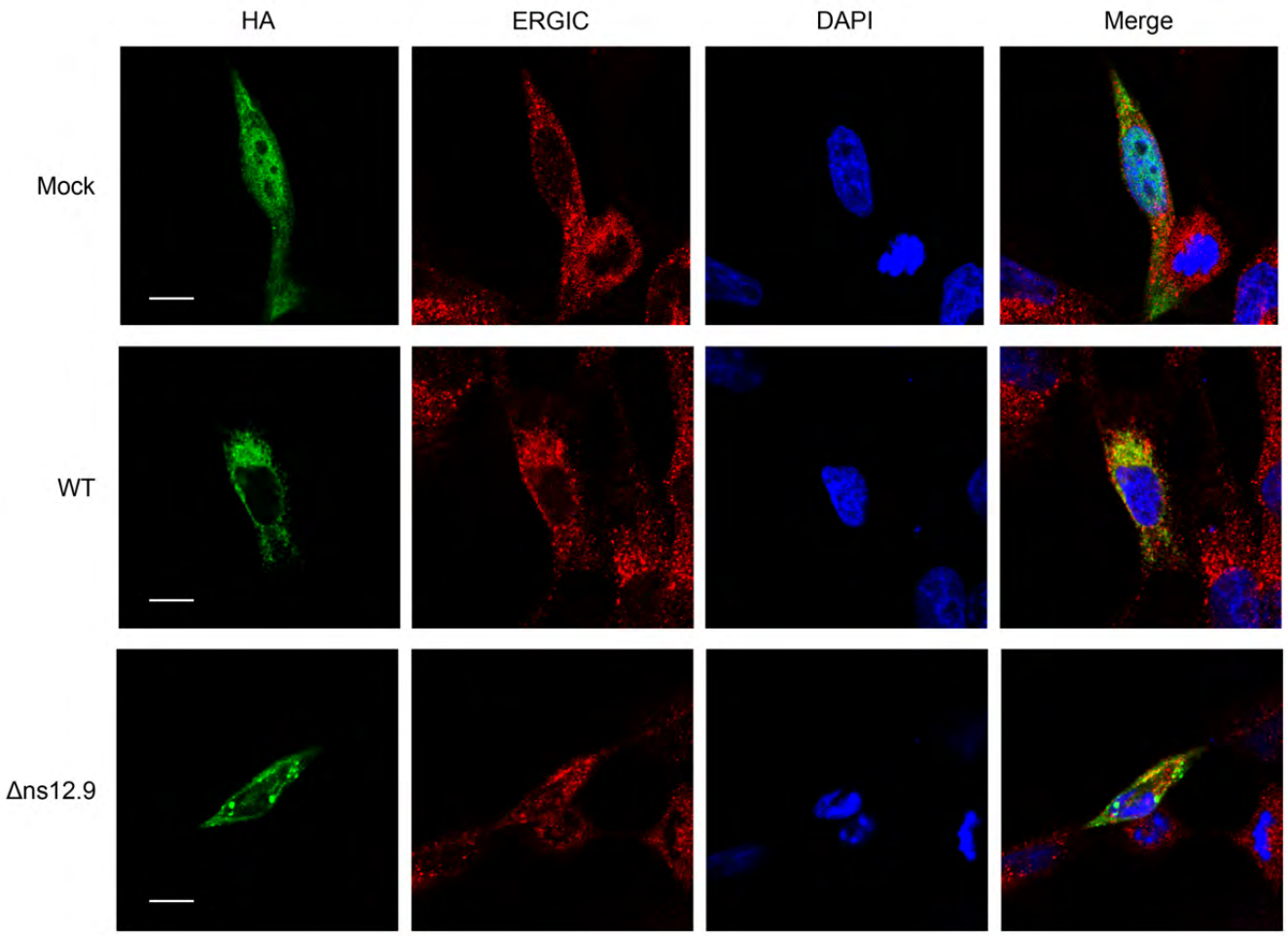

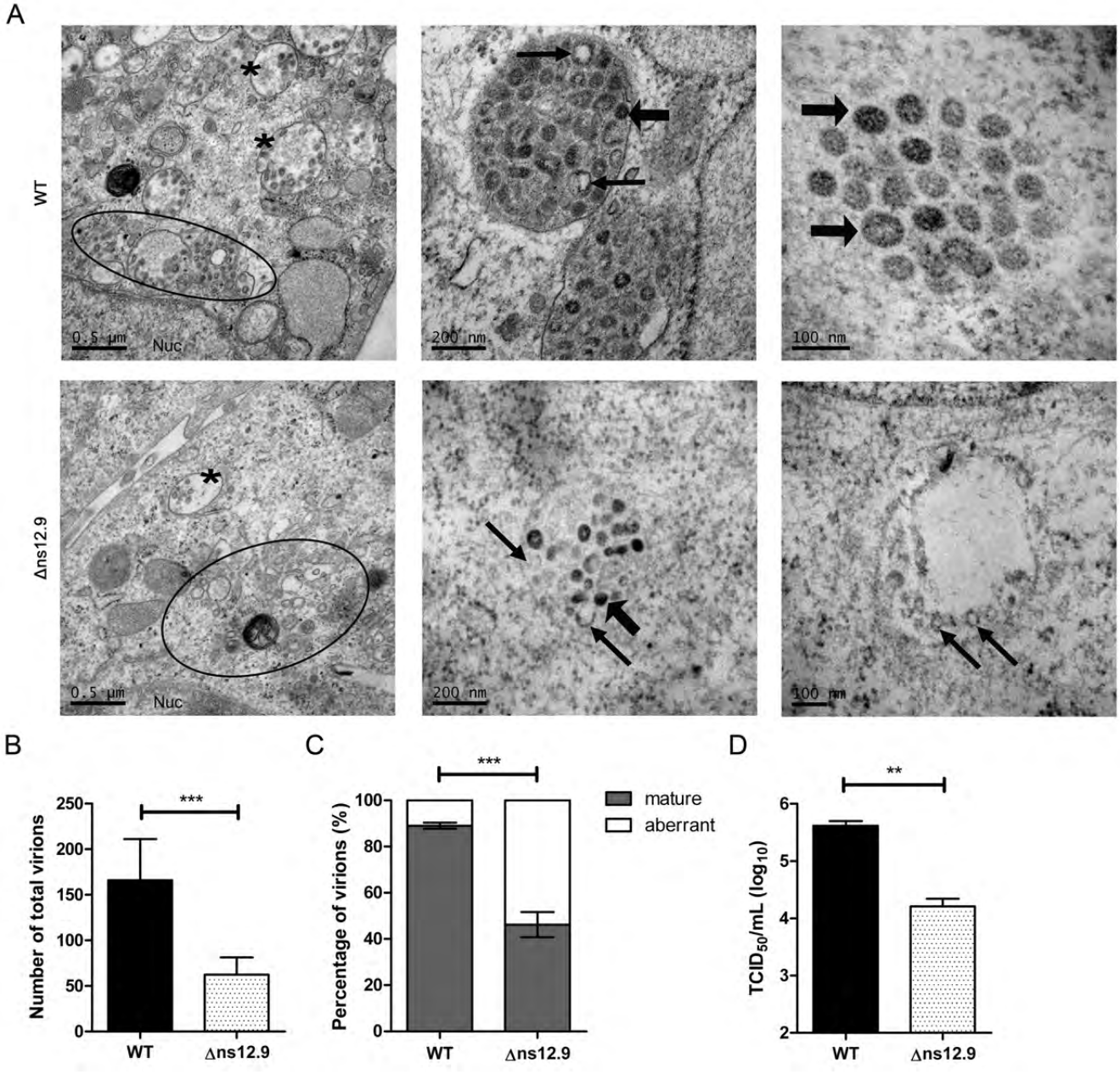

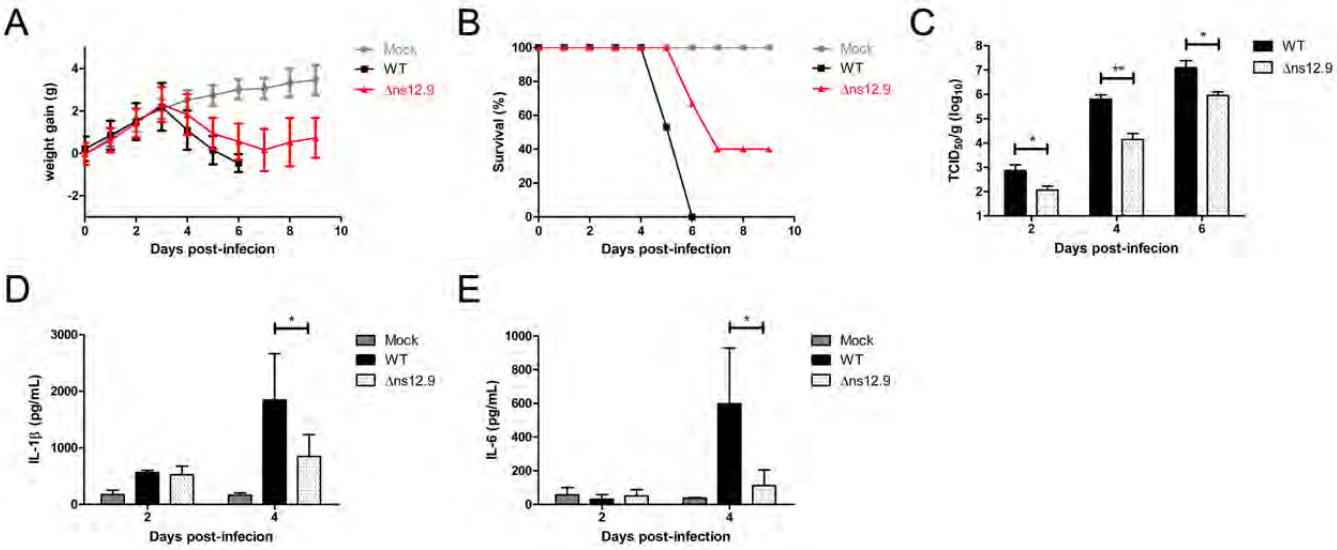

TABLE 1 Primers used to test the copies of genomic RNA and sgmRNAs by qRT-PCR

Primer	Sequence (5'-3')
OC43-RT-F	GTTTGAGGACGCAGAGGAGAAG
OC43-RT-R	AAGAAGTCGGCGACAATCCACC
Leader-F	CATCCCGCTTCACTGATCTCTTG
Rep1a/b-sgmRNA-R	CGCCCACAAGCATAGATTACAGG
ns2-sgmRNA-R	AACCCTGAAAATGGGTAAGTGG
HE-sgmRNA-R	CGAAACAACATTGGTAGGAGGGT
S-sgmRNA-R	TAGGAGGAGGACCGGTGTCTTTATC
ns12.9-sgmRNA-R	ACGGAGATATTTCTTCTCAGGTCT
E-sgmRNA-R	TTATTTGCCCCACATACCACACAG
M-sgmRNA-R	TTTAATAGCTTCATCAGCAGTCCAG
N-sgmRNA-R	CCCACTTGAGGATGCCATTACCAG
β-actin-F	ACGTTGCTATCCAGGCTGTG
β-actin-R	GAGGGCATACCCCTCGTAGA